Hindawi
Mathematical Problems in Engineering
Volume 2019, Article ID 5234642, 9 pages
https://doi.org/10.1155/2019/5234642

Research Article

Mechanism of Fracturing in Shaft Lining Caused by High-Pressure Pore Water in Stable Rock Strata

Jihuan Han,[1] **Jiuqun Zou**,[1] **Weihao Yang**,[1,2] **and Chenchen Hu**[1]

[1]*State Key Laboratory for Geomechanics and Deep Underground Engineering, China University of Mining and Technology, Xuzhou 221116, Jiangsu Province, China*
[2]*School of Mechanics and Civil Engineering, China University of Mining and Technology, Xuzhou 221116, Jiangsu Province, China*

Correspondence should be addressed to Weihao Yang; whyang@cumt.edu.cn

Received 8 March 2019; Revised 3 June 2019; Accepted 11 June 2019; Published 26 June 2019

Guest Editor: Raffaele Albano

With the increase in shaft depth, the problem of cracks and leakage in single-layer concrete lining in porous water-rich stable rock strata has become increasingly clear, in which case the mechanism of fracturing in shaft lining remains unclear. Considering that the increase in pore water pressure can cause rock mass expansion, this paper presents the concept of hydraulic expansion coefficient. First, a cubic model containing spherical pores is established for studying hydraulic expansion, and the ANSYS numerical simulation, a finite element numerical method, was used for calculating the volume change of the model under the pore water pressure. By means of the multivariate nonlinear regression method, the regression equation of the hydraulic expansion coefficient is obtained. Second, based on the hydraulic expansion effect on the rock mass, an interaction model of pore water pressure–porous rock–shaft lining is established and further solved. Consequently, the mechanism of fracturing in shaft lining caused by high-pressure pore water is revealed. The results show that the hydraulic expansion effect on the surrounding rock increases with its porosity and decreases with its elastic modulus and Poisson's ratio; the surrounding rock expansion caused by the change in pore water pressure can result in the outer edge of the lining peeling off from the surrounding rock and tensile fracturing at the inner edge. Therefore, the results have a considerable guiding significance for designing shaft lining through porous water-rich rock strata.

1. Introduction

In recent years, with the implementation of China's western development strategy, the abundant coal resources in some water-rich bedrock areas (Shaanxi, Ningxia, Gansu, Inner Mongolia, etc.) have been mined on a large scale [1]. Since the shaft is the passageway of mine production, the shaft lining should be designed with sufficient strength, rigidity, and waterproof performance to meet the requirements of safety, sealing, and durability. However, with the increase in coal mining depth, the non-mining-related deformation and fracture of the shaft lining under the action of high water pressure is still very serious. At present, scholars at home and abroad have carried out a lot of considerable research on shaft fracture caused by groundwater activities. Regarding the study topic on groundwater seepage, Farmer [2] studied the hydrostatic stresses acting on shaft lining based on the theory of surrounding rock permeability. Bear [3] carried out a microscopic study on the seepage mechanism, indicating that the change in pore shape is a sensitive factor that causes permeability coefficient changes. Bruno [4] studied the effect of pore pressure on the tensile fracture of rock on the basis of Biot theory and noted the importance of fluid-solid coupling in hydraulic fracturing. Zimmerman [5] briefly deduced the linear porous-elasticity and thermoelastic equation by using the three-dimensional fluid-solid coupling seepage model. Jiang [6] used a high-pressure permeability test to simulate the deformation law of rock mass fracturing under the action of pore water pressure. Regarding the study topic on hydrophobic settlement, Lou [7] derived a general formula for calculating the additional stress in the shaft lining based on the drainage consolidation theory. According to the principle of superposition and strain compatibility, Yang [8] derived the theoretical solution of vertical additional stress

on the shaft lining by using a numerical method. Wang [9] obtained the additional stress value at complex alluvium strata by the negative friction coefficient between the shaft lining and surrounding rock. Zhang [10] studied the fluid-solid coupling numerical simulation of sharp severely aquifer drainage in underground mining and analyzed the influence of drainage location and drainage rate on the stability of shaft lining. Regarding the study on unstable rock strata, Sun [11] simulated and analyzed the deformation and stress characteristics of surrounding rock and shaft lining under the interactive geological conditions of soft and hard rock strata, and the conclusion that the shear failure occurred in shaft lining under the inhomogeneous pressure of surrounding rock was obtained. In addition, Yang [12] deduced the elastic approximate stress and displacement solution of irregular inclined shaft lining subjected to water pressure and proposed the optimal design for inclined shaft lining. Meng [13] classified and studied the constructing techniques for the inclined shaft penetrating the drift sand stratum, and the problems such as the stability of inclined shaft structure and the sealing of water and sand were solved. It is well known that shaft lining in porous water-rich rock strata is constructed by the temporary drainage method or the frozen water method. When the drainage or freezing is stopped, the pore water pressure of the surrounding rock will rise, and at this time, cracking and leakage of lining often occurs. However, no leakage occurs before the shaft lining fractures, inhibiting seepage in the surrounding rock. Additionally, the theory of vertical additional stress caused by mining hydrophobic settlement is applicable to mainly alluvium. Clearly, although some existing theories have matured, the fracture mechanism of shaft lining in high-pressure water-rich stable rock strata has not been clarified.

Based on the compressive and expansive deformation properties of the porous media under the action of stress, in analogy with the coefficient of thermal expansion, this paper defines the linear expansion coefficient of the rock caused by unit pore water pressure as the hydrostatic expansion coefficient, which is expressed as α. With the advantage of solving complex problems that cannot be solved by theoretical and experimental research and having the characteristics suitable for any problem geometry and boundary conditions [14], the finite element numerical method has become one of the most effective methods to solve scientific and engineering problems. Therefore, the ANSYS numerical simulation is adopted to obtain the volume change of the cubic model under the pore water pressure. Based on the calculation results, the approximate analytical solution of the hydraulic expansion coefficient is derived by means of the multivariate nonlinear regression method. By comprehensively analyzing the influence of various factors on the shaft lining stress, the mechanism of fracturing in shaft lining due to high-pressure pore water is clarified, providing an effective and scientific basis for lining safety.

2. Hydraulic Expansion Coefficient Solution

2.1. Basic Assumptions. (1) The rock mass is composed of an infinite number of identical cubic microunits containing spherical pores of equal diameter, and the rock is a homogeneous and isotropic linear elastic medium.

(2) The effect of pore water pressure on a microunit can be regarded as free expansion, and the effect on the rock is the superposition of the expansive effect of each microunit [15].

The elastic modulus, Poisson's ratio, and porosity of the cubic model containing spherical pores are expressed by E_0, $\mu_{0,}$ and n_0, respectively. Since the elastic modulus reflects the degree of rock elastic deformation, E_0 is clearly inversely proportional to α. According to the basic assumptions, the hydraulic expansion coefficient of the entire porous water-rich rock is equal to that of any single cubic microunit containing spherical pores under conditions of a free boundary. Assuming α_v is the volumetric hydraulic expansion coefficient of the rock, $\alpha_v = 3\alpha$ when the infinitesimal of higher order is ignored. Considering that n_0 and μ_0 are both dimensionless parameters, then αE_0 can be studied as dimensionless. When the compressive stress is specified as positive, the following equations can be derived from the theory of elastic mechanics.

$$\widetilde{\alpha} = \frac{\Delta\widetilde{V}}{\left(3\Delta\widetilde{p}_w\right)}, \tag{1}$$

$$n_0 = \frac{\pi\widetilde{r}_0^3}{6}, \tag{2}$$

$$\begin{aligned} \widetilde{\alpha} &= \alpha E_0, \\ \Delta\widetilde{p}_w &= \frac{\Delta p_w}{E_0}, \\ \Delta\widetilde{V} &= \frac{\Delta V}{V}, \\ \widetilde{r}_0 &= \frac{r_0}{a} < 1, \end{aligned} \tag{3}$$

where V is the total volume of the cubic model, p_w is the pore water pressure, r_0 is the pore radius, and a is the half length of the microunit.

2.2. Solution Result. According to the characteristics of the solution model, a 1/8 cubic model containing spherical pore is established by ANSYS numerical simulation, and the volume change in the model with different values of n_0 and μ_0 under the action of pore water pressure is calculated. When $\Delta\widetilde{p}_w = 0.1$, taking n_0=0.1, μ_0=0.2 as an example, the model after mesh generation is shown in Figure 1, and the equivalent displacement cloud of the model after solution is shown in Figure 2.

By means of the same method, $\Delta\widetilde{V}$ can be calculated with different parameters of cubic model, as shown in Figure 3.

Based on the changing laws of the data in Figure 3, the multivariate nonlinear regression method is adopted to obtain the expression of $\Delta\widetilde{V}$ for n_0 and μ_0, which satisfies that when $n_0 \approx 0$, $\Delta\widetilde{V} \approx 0$. Toward this goal, the objective function can be expressed as

$$\Delta\widetilde{V} = \frac{\Delta\widetilde{p}_w n_0 \left(\lambda_1 n_0^2 + \lambda_2 n_0 + \lambda_3\right)\left(\lambda_4 - \mu_0\right)}{\left(\lambda_5 - n_0\right)}, \tag{4}$$

Table 1: Regression coefficients values.

λ_1	λ_2	λ_3	λ_4	λ_5	R^2
-3.509	-0.261	1.952	1.087	0.505	0.9995

Note: R^2 is the goodness of fit.

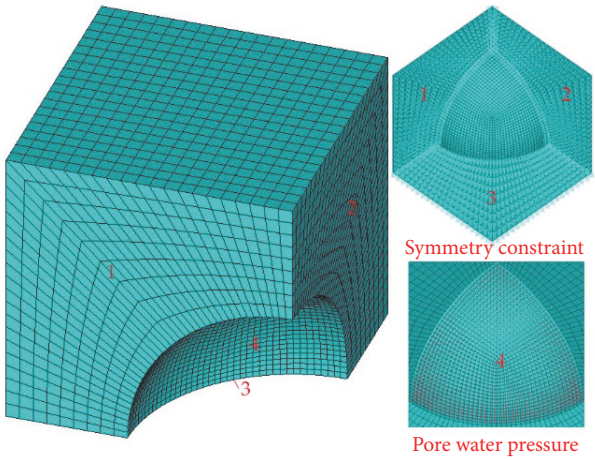

Figure 1: Mesh generation.

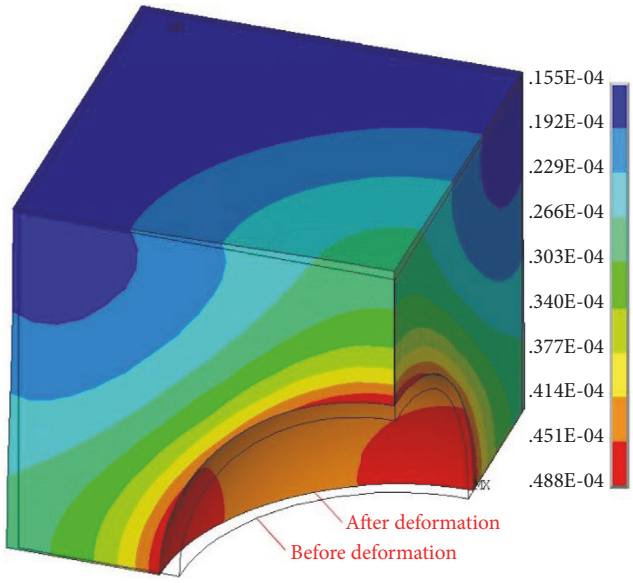

Figure 2: Equivalent displacement cloud (deformation scale factor: 1000).

where n_0 satisfies the general rock porosity value; i.e., $n_0 < 0.5$, $\lambda_1, \lambda_2, \lambda_3, \lambda_4$, and λ_5 are the regression coefficients, the values of which are shown in Table 1.

Substitute (4) into (1). Then,

$$\widetilde{\alpha} = \frac{n_0\left(0.651 - 0.087n_0 - 1.17n_0^2\right)}{0.505 - n_0}\left(1.087 - \mu_0\right). \quad (5)$$

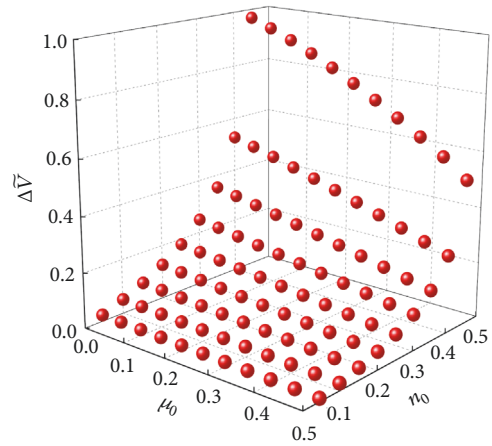

Figure 3: Values of $\Delta\widetilde{V}$ with different parameters.

3. The Variation Law of the Coefficient of Hydraulic Expansion

3.1. Regular Analysis. Analysis of the relationship between the hydraulic expansion coefficient and the various parameters is helpful to better understand the influence law of hydraulic expansion on underground structures in different water-rich rock strata and has an important guiding significance for mitigation of the shaft lining fracture problem. Therefore, the partial derivatives of n_0 and μ_0 for (5) are solved, and (6) and (7) are always satisfied.

$$\frac{\partial\widetilde{\alpha}}{\partial n_0} > 0, \quad (6)$$

$$\frac{\partial\widetilde{\alpha}}{\partial \mu_0} < 0, \quad \frac{\partial^2\widetilde{\alpha}}{\partial \mu_0^2} = 0. \quad (7)$$

The results show that the hydraulic expansion coefficient increases with n_0 and linearly decreases with μ_0.

3.2. Influence of Pore Shape on Hydraulic Expansion Effect. Rock is a typical porous medium, in which the internal pores are not a sphere but an irregular space with various forms and a fractal dimension [16]. Therefore, an equal-porosity cubic model with a regular N-polyhedron is adopted to analyze the influence of pore shape on the hydrostatic expansion effect, where N=4, 6, 8, 12, 20, and ∞ (sphere). If the hydraulic expansion coefficient of the model with a regular N-polyhedron pore is expressed as α_N, then $\widetilde{\alpha}_N$ =

Table 2: Fitting coefficient values.

Curve Num.	n_0	η_1	η_2	R^2	Adj. R^2
1	0.02	0.651	10.920	0.9837	0.9796
2	0.06	0.669	8.877	0.9831	0.9789
3	0.10	0.719	8.304	0.9910	0.9887
4	0.20	1.031	7.003	0.9818	0.9772
5	0.30	1.432	7.896	0.9847	0.9808
6	0.40	1.878	7.124	0.9856	0.9809

Note: Adj. R^2 is the goodness of fit after correction.

Table 3: The range value of $f(n_0, N)$.

N	4	6	8	12	20
$f(n_0, N)$	3.0~7.8	1.8~3.0	1.5~2.0	1.2~1.6	1.0~1.4

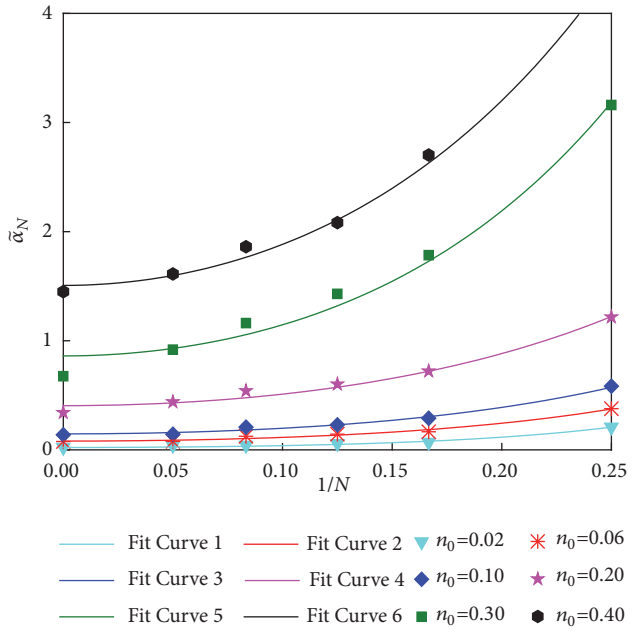

Figure 4: The relationship between $\tilde{\alpha}_N$ and $1/N$.

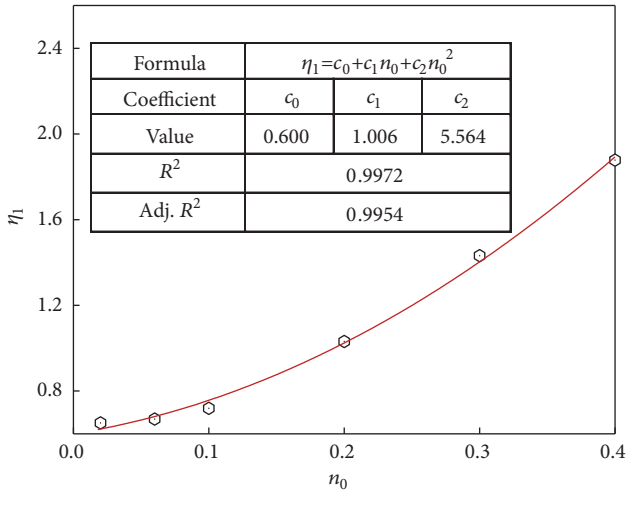

Figure 5: The expression of η_1.

$\alpha_N E_0$. Taking μ_0=0.2 as an example, the relationship between $\tilde{\alpha}_N$ and $1/N$ at different n_0 values can be obtained by the ANSYS numerical simulation (see Figure 4). The expressions of the fitting function in Figure 4 can be expressed in the form of (8), and the corresponding fitting coefficient values are shown in Table 2.

As shown in Figure 4, $\tilde{\alpha}_N$ increases with n_0 and decreases with N. The hydraulic expansion coefficient of the model containing the tetrahedral pore is the largest, while that of the model containing the spherical pore is the smallest.

$$\tilde{\alpha}_N = n_0\eta_1\left[\exp\left(\frac{\eta_2}{N}\right) + \exp\left(\frac{-\eta_2}{N}\right)\right], \tag{8}$$

where η_1 and η_2 are both functions in terms of n_0.

Based on the data in Table 2, the polynomial regression formulae of η_1 and η_2 can be calculated, as shown in Figures 5 and 6, respectively.

Since both $\tilde{\alpha}_N$ and $\tilde{\alpha}$ are functions of regarding n_0 and N, the function $f(n_0, N)$ can be used to represent the value of $\tilde{\alpha}_N/\tilde{\alpha}$. When μ_0=0.2, the expression of $f(n_0, N)$ can be derived from (5) and (8) as follows:

$$f(n_0, N) = \frac{(0.505 - n_0)\,\eta_1\left[\exp(\eta_2/N) + \exp(-\eta_2/N)\right]}{0.577 - 0.077n_0 - 1.038n_0^2} \tag{9}$$

The value of $f(n_0, N)$ for different rock porosities can be solved by (9). Therefore, when μ_0 is between 0.1 and 0.3 and n_0 is between 0.02 and 0.4, the range of $f(n_0, N)$ can be obtained, as seen in Table 3.

As seen in Table 3, the hydraulic expansion coefficient of the model containing regular polyhedral pores is approximately (1.0~7.8) α and decreases with the number of pore faces.

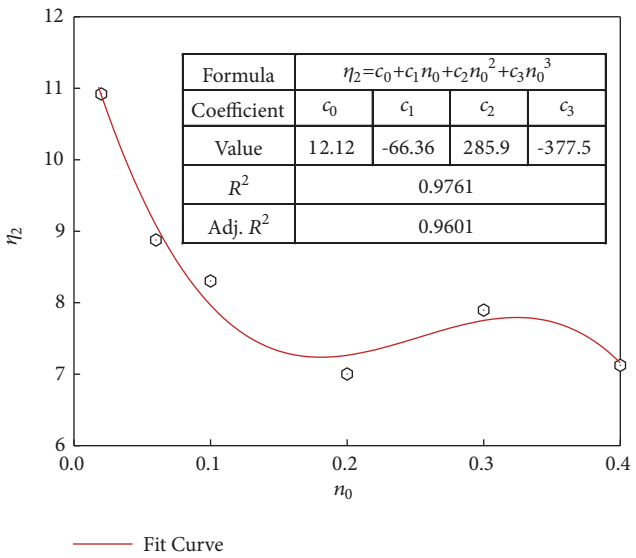

Formula	$\eta_2=c_0+c_1n_0+c_2{n_0}^2+c_3{n_0}^3$			
Coefficient	c_0	c_1	c_2	c_3
Value	12.12	-66.36	285.9	-377.5
R^2	0.9761			
Adj. R^2	0.9601			

FIGURE 6: The expression of η_2.

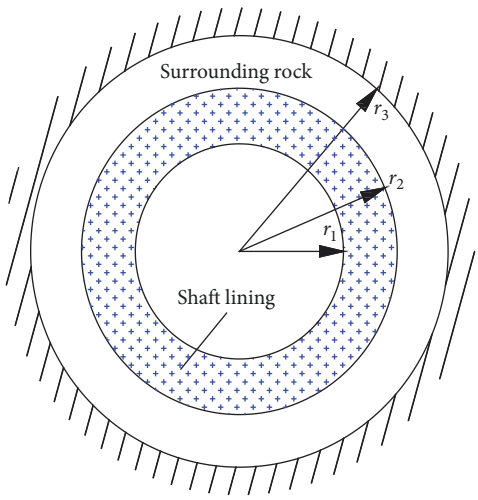

FIGURE 7: Stress analysis model of shaft lining.

4. Mechanism of Shaft Lining Fracture Analysis

4.1. Stress and Displacement Solution

4.1.1. Basic Assumptions. In the absence of water, the elastic moduli of the surrounding rock and the shaft lining are E_1 and E_2, the corresponding Poisson's ratios are μ_1 and μ_2, the corresponding porosities are n_1 and n_2, respectively, and the porosity of the contact surface between the surrounding rock and the shaft lining is n_3.

According to the nature of the problem, the following assumptions are made.

(1) The elastic modulus and Poisson's ratio of the surrounding rock mass and the rock matrix approximately satisfy the linear relations as follows:

$$E_1 = E_0\left(1 - k_1 n_1\right), \tag{10}$$

$$\mu_1 = \mu_0\left(1 - k_2 n_1\right), \tag{11}$$

where k_1 and k_2 are constants related to pore shape, for spherical pores [17]: k_1=2.08, and k_2=0.345.

(2) The porosity of contact surface n_3 can be calculated according to the probability statistical method, namely, $n_3=n_1+n_2-n_1n_2$.

(3) The shaft lining is a homogeneous, continuous, and isotropic linear elastic medium.

(4) The expansion effect of the pore water pressure on the surrounding rock can be equivalent to the volume expansion of elastomer, which is similar to the thermal expansion.

(5) The inner and outer radii of the shaft lining are r_1 and r_2, respectively, and the inner and outer radii of the surrounding rock are r_2 and r_3, respectively. The outer boundary of the surrounding rock is fixed, as shown in Figure 7.

Assume that the interaction force between the surrounding rock and the shaft lining under the action of pore water pressure is a compressive stress, and the stress direction is defined as positive. The radial displacement is expressed by u_r, and the radial stress and circumferential stress are expressed by σ_r and σ_θ, respectively, and the radial strain and circumferential strain are expressed by ε_r and ε_θ, respectively. The total stress at the interface is p_0, and the effective stress is p_1. The bonding strength is f_1, the uniaxial compressive design strength and the uniaxial tensile design strength of the concrete are f_c and f_t, respectively, and the compressive design strength and the tensile design strength of the reinforcement are f_y' and f_y, respectively. To facilitate the analysis, the relevant parameters are dimensionless as follows:

$$\mathrm{d}\widetilde{\sigma}_r = \frac{\mathrm{d}\sigma_r}{\Delta p_w},$$

$$\mathrm{d}\widetilde{u}_r = \frac{\mathrm{d}u_r}{\mathrm{d}r},$$

$$\mathrm{d}\widetilde{r} = \frac{\mathrm{d}r}{r},$$

$$\widetilde{u}_r = \frac{u_r}{r},$$

$$\widetilde{\sigma}_r = \frac{\sigma_r}{\Delta p_w},$$

$$\widetilde{\sigma}_\theta = \frac{\sigma_\theta}{\Delta p_w},$$

$$\widetilde{r}_{12} = \frac{r_1}{r_2},$$

$$\widetilde{r}_{23} = \frac{r_2}{r_3},$$

$$\widetilde{E}_{12} = \frac{E_1}{E_2},$$

$$\widetilde{\alpha}_1 = \alpha E_1,$$

$$\begin{aligned}
\widetilde{p}_0 &= \frac{p_0}{\Delta p_w},\\
\widetilde{p}_1 &= \frac{p_1}{\Delta p_w},\\
\widetilde{f}_1 &= \frac{f_1}{\Delta p_w},\\
\widetilde{f}_c &= \frac{f_c}{\Delta p_w},\\
\widetilde{f}_t &= \frac{f_t}{\Delta p_w},\\
\widetilde{f}'_y &= \frac{f'_y}{\Delta p_w},\\
\widetilde{f}_y &= \frac{f_y}{\Delta p_w},\\
\Delta\widetilde{p}_{w1} &= \frac{\Delta p_w}{E_1},\\
\Delta\widetilde{p}_{w2} &= \frac{\Delta p_w}{E_2}.
\end{aligned} \tag{12}$$

4.1.2. Stress and Displacement Solution in the Surrounding Rock Zone. The equations of equilibrium in the surrounding rock zone can be expressed as [18]

$$\frac{\mathrm{d}\widetilde{\sigma}_r}{\mathrm{d}\widetilde{r}} + \widetilde{\sigma}_r - \widetilde{\sigma}_\theta = 0. \tag{13}$$

The equations of geometry for the axisymmetric plane strain problem can be written as

$$\begin{aligned}
\varepsilon_r &= \mathrm{d}\widetilde{u}_r,\\
\varepsilon_\theta &= \widetilde{u}_r.
\end{aligned} \tag{14}$$

The equations of constitution in the surrounding rock zone under the action of water pressure expansion can be expressed as

$$\varepsilon_r = \Delta\widetilde{p}_{w1}\left(1+\mu_1\right)\left[\left(1-\mu_1\right)\widetilde{\sigma}_r - \mu_1\widetilde{\sigma}_\theta + \widetilde{\alpha}_1\right], \tag{15}$$

$$\varepsilon_\theta = \Delta\widetilde{p}_{w1}\left(1+\mu_1\right)\left[\left(1-\mu_1\right)\sigma_\theta - \mu_1\sigma_r + \widetilde{\alpha}_1\right]. \tag{16}$$

The boundary conditions of the surrounding rock can be expressed as

$$\widetilde{\sigma}_r\big|_{r=r_2} = \widetilde{p}_0, \tag{17}$$

$$\widetilde{u}_r\big|_{r=r_3} = 0. \tag{18}$$

According to (13)~(18), the analytical solutions of the stress and displacement in the surrounding rock zone can be obtained as

$$\widetilde{\sigma}_r = \frac{\left(1-2\mu_1\right)\widetilde{p}_0 + \widetilde{\alpha}_1}{1+\left(1-2\mu_1\right)/\widetilde{r}_{23}^2}\left(\frac{1}{1-2\mu_1} + \frac{r_3^2}{r^2}\right) - \frac{\widetilde{\alpha}_1}{1-2\mu_1}, \tag{19}$$

$$\widetilde{\sigma}_\theta = \frac{\left(1-2\mu_1\right)\widetilde{p}_0 + \widetilde{\alpha}_1}{1+\left(1-2\mu_1\right)/\widetilde{r}_{23}^2}\left(\frac{1}{1-2\mu_1} - \frac{r_3^2}{r^2}\right) - \frac{\widetilde{\alpha}_1}{1-2\mu_1}, \tag{20}$$

$$\widetilde{u}_r = \Delta\widetilde{p}_{w1}\left(1+\mu_1\right)\frac{\left(1-2\mu_1\right)\widetilde{p}_0 + \widetilde{\alpha}_1}{1+\left(1-2\mu_1\right)/\widetilde{r}_{23}^2}\left(1 - \frac{r_3^2}{r^2}\right). \tag{21}$$

4.1.3. Stress and Displacement Solution in the Shaft Lining Zone. The equations of equilibrium and geometry in the shaft lining zone are the same as those in the surrounding rock zone, and the equations of constitution can be expressed as

$$\varepsilon_r = \Delta\widetilde{p}_{w2}\left[\left(1-\mu_2^2\right)\widetilde{\sigma}_r - \mu_2\left(1+\mu_2\right)\widetilde{\sigma}_\theta\right], \tag{22}$$

$$\varepsilon_\theta = \Delta\widetilde{p}_{w2}\left[\left(1-\mu_2^2\right)\widetilde{\sigma}_\theta - \mu_2\left(1+\mu_2\right)\widetilde{\sigma}_r\right]. \tag{23}$$

The boundary conditions of the shaft lining can be expressed as

$$\widetilde{\sigma}_r\big|_{r=r_1} = 0, \tag{24}$$

$$\widetilde{\sigma}_r\big|_{r=r_2} = \widetilde{p}_0. \tag{25}$$

The analytical solutions of the stress and displacement in the shaft lining zone can be derived as

$$\widetilde{\sigma}_r = \frac{1-r_1^2/r^2}{1-\widetilde{r}_{12}^2}\widetilde{p}_0, \tag{26}$$

$$\widetilde{\sigma}_\theta = \frac{1+r_1^2/r^2}{1-\widetilde{r}_{12}^2}\widetilde{p}_0, \tag{27}$$

$$\widetilde{u}_r = \Delta\widetilde{p}_{w2}\widetilde{p}_0\left(1+\mu_2\right)\frac{1-2\mu_2+r_1^2/r^2}{1-\widetilde{r}_{12}^2}. \tag{28}$$

4.2. Stress Analysis at the Interface between the Surrounding Rock and Shaft Lining

4.2.1. Total Stress Analysis. Considering the conditions of single-valued displacement at the interface between the surrounding rock and the shaft lining, $\widetilde{p}_0$ can be solved by (21) and (28) as follows:

$$\widetilde{p}_0 = \frac{\widetilde{\alpha}_1}{\left[1-2\mu_1+\left(\left(1+\mu_2\right)/\left(1+\mu_1\right)\right)\left(\left(1-2\mu_2+\widetilde{r}_{12}^2\right)\left(1-2\mu_1+\widetilde{r}_{23}^2\right)/\left(1-\widetilde{r}_{12}^2\right)\left(1-\widetilde{r}_{23}^2\right)\right)\widetilde{E}_{12}\right]}. \tag{29}$$

The partial derivative of $\widetilde{r}_{23}$ for $\widetilde{p}_0$ is

$$\frac{\partial \widetilde{p}_0}{\partial \widetilde{r}_{23}} < 0. \tag{30}$$

According to (30), the smaller the value of $\widetilde{r}_{23}$ is, the larger the value of $\widetilde{p}_0$ is. Therefore, when the outer boundary of the surrounding rock is farther from the interface between the lining and the surrounding rock, the interaction force at the interface is greater under the unit pore water pressure. When $\widetilde{r}_{23} \approx 0$, the interaction force is a constant value equal to

$$\widetilde{p}_0 = \frac{\widetilde{\alpha}_1}{\left\{(1-2\mu_1)\left[1+\left((1+\mu_2)/(1+\mu_1)\right)\left((1-2\mu_2+\widetilde{r}_{12}^2)/(1-\widetilde{r}_{12}^2)\right)\widetilde{E}_{12}\right]\right\}}. \tag{31}$$

By analyzing (31), it can be found that

(1) when $\widetilde{E}_{12} \approx \infty$, $\widetilde{p}_0 \approx 0$;

(2) when $\widetilde{E}_{12} \approx 0$, $\widetilde{p}_0 = \widetilde{\alpha}_1/(1-2\mu_1)$;

(3) when $\widetilde{r}_{12} \approx 1$, $\widetilde{p}_0 \approx 0$.

The results show that when the elastic modulus of the surrounding rock is too large compared with the shaft lining, p_0 is close to 0; otherwise, p_0 is constant. Additionally, when the lining thickness is very small, p_0 approaches 0; when the pore water pressure increases ($\Delta p_w > 0$), p_0 is a compressive stress, and a compressive fracture forms at the inner edge of the shaft lining. Finally, when the pore water pressure decreases ($\Delta p_w < 0$), p_0 is a tensile stress, and a tensile fracture forms at the inner edge of the shaft lining.

4.2.2. Effective Stress Analysis. According to the composition of the stress at the contact surface between the surrounding rock and the shaft lining, the effective stress (or skeleton stress) at the contact surface can be expressed as

$$\widetilde{p}_1 = \widetilde{p}_0 - n_3. \tag{32}$$

By analyzing (32), it can be found that

(1) when $\widetilde{p}_0 = n_3$, then $\widetilde{p}_1 = 0$; that is, the contact skeleton stress is equal to 0;

(2) when the pore water pressure increases, if $\widetilde{p}_0 < n_3$, then $\widetilde{p}_1 < 0$, and the skeleton stress at contact surface is tensile stress; if $\widetilde{p}_0 > n_3$, then $\widetilde{p}_1 > 0$, and the skeleton stress at contact surface is compressive stress;

(3) when the pore water pressure decreases, if $\widetilde{p}_0 < n_3$, then $\widetilde{p}_1 < 0$, and the skeleton stress at contact surface is compressive stress; if $\widetilde{p}_0 > n_3$, then $\widetilde{p}_1 > 0$, and the skeleton stress at contact surface is tensile stress.

The results show that when the skeleton stress at the contact surface is subjected to tensile stress, the shaft lining has a risk of peeling off the surrounding rock.

4.3. Shaft Lining Fracture Condition Analysis

4.3.1. Fracture Condition at Inner Edge of Shaft Lining. When p_0 is the compressive stress, the inner edge of the shaft lining is in compression. According to the Code [19], the compressive failure condition at the inner edge of the shaft lining is

$$\widetilde{\sigma}_\theta\big|_{r=r_1} > \eta \widetilde{f}_c + \nu \widetilde{f}'_y, \tag{33}$$

where η is the improvement coefficient of the concrete strength under multiaxial stress, η is related to σ_θ and σ_r (in general, $\eta = 1.2$), and ν is the minimum steel content.

When p_0 is a tensile stress, the inner edge of the shaft lining is in tension. According to the Code [20], the tensile failure condition at the inner edge of the shaft lining is

$$\widetilde{\sigma}_\theta\big|_{r=r_1} > \left|\eta \widetilde{f}_t + \nu \widetilde{f}_y\right|. \tag{34}$$

4.3.2. Stripping Condition at Outer Edge of Shaft Lining. To avoid the hydrostatic action of groundwater on the entire outside surface of the shaft lining, there must be a certain bonding strength between the shaft lining and surrounding rock to ensure that the two are not separated. Therefore, when the contact surface skeleton is subjected to tension, the condition for peeling of the outer edge of the shaft lining away from the surrounding rock is

$$\left|\widetilde{p}_1\right| > \left|\widetilde{f}_1\right|. \tag{35}$$

The Code [20] stipulates that the bonding strength of shotcrete should be no less than 0.8 MPa with Class I and Class II surrounding rock and should be no less than 0.5 MPa with Class III surrounding rock, respectively. However, the bonding strength between the pouring concrete and the surrounding rock is less than these values. In fact, the maximum bonding strength between the shaft lining and the surrounding rock in engineering is less than 1 MPa.

5. Engineering Example

A shaft passes through water-rich bedrock strata with Class III surrounding rock. The radius of the shaft is r_1=3 m, and the shaft lining is made of C60 concrete and HRB335 steel, that is, f_c=27.5 MPa, f_t=2.04 MPa, f_y=300 MPa, and f'_y = 300 MPa. The other parameters are as follows: E_0=15 GPa, E_2=36 GPa, μ_0=0.16, μ_2=0.2, n_1=0.15, n_2=0.12, ν=0.2%, f_1=0.8 MPa. For a change in groundwater level in the water-rich bedrock strata of 500 m, the fracturing in the lining with different thicknesses is shown in Figures 8 and 9.

The calculation results show that $\widetilde{p}_1 < 0$. Figures 8 and 9 show that when the water level rises, there is no compressive failure at the inner edge of the shaft lining, while stripping failure occurs at the outer edge of the shaft lining when $\widetilde{r}_{12} > 0.918$; when the water level drops, only the inner edge of the shaft lining undergoes tensile fracturing.

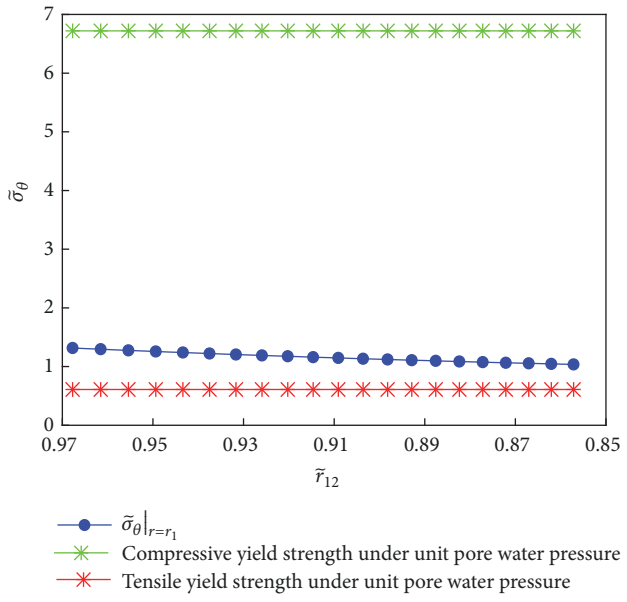

Figure 8: Fracture condition at inner edge of shaft lining.

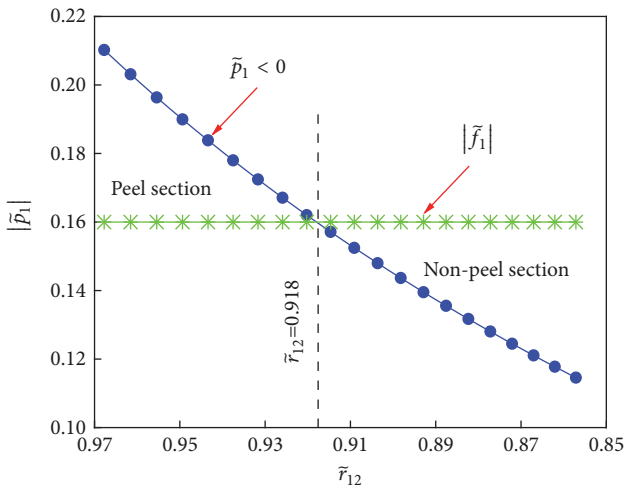

Figure 9: Stripping condition at outer edge of shaft lining.

To further study the relationship between the stress and the deformation at the outer edge of the shaft lining, the lateral stiffness coefficient K_c of the lining can be calculated from (28) and (32), which can be derived as

$$K_c = \frac{p_0}{u_r|_{r=r_2}} = \frac{\left(1-\tilde{r}_{12}^2\right)}{\left(1+\mu_2\right)\left(1-2\mu_2+\tilde{r}_{12}^2\right)}\frac{E_2}{r_2}. \quad (36)$$

According to (36), the values of K_c with different thicknesses are shown in Figure 10.

As shown in Figure 10, K_c decreases approximately linearly with $\tilde{r}_{12}$, indicating that the increase in shaft lining thickness can effectively improve the lateral stiffness coefficient.

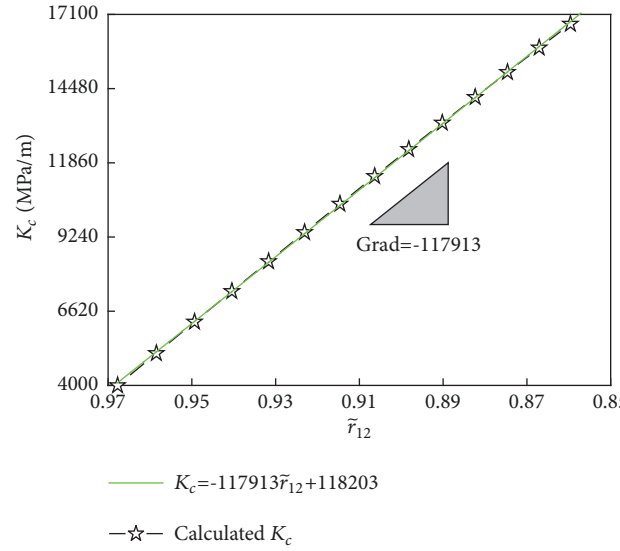

Figure 10: Values of K_c with different $\tilde{r}_{12}$.

6. Conclusions

Based on the cubic model of hydraulic expansion containing a spherical pore, its volume change is calculated by the ANSYS numerical simulation, and the approximate analytical solution of the hydraulic expansion coefficient is obtained by the multivariate nonlinear regression method. Finally, the mechanism of fracturing in single-layer concrete lining caused by high-pressure pore water in stable rock strata is revealed by analyzing the interaction between the pore water pressure and the porous rock and shaft lining, and the following conclusions are obtained.

(1) The hydraulic expansion effect increases with the porosity of the surrounding rock and decreases with the elastic modulus and Poisson's ratio of the surrounding rock. Therefore, by reducing the porosity and improving the strength of the surrounding rock, the expansion effect of the surrounding rock on shaft lining can be weakened.

(2) The mechanism of fracturing in shaft lining in water-rich bedrock strata is as follows: the hydraulic expansion effect on the surrounding rock may lead to stripping failure at the outer edge or tensile failure at the inner edge of the shaft lining.

(3) When designing the shaft lining of water-rich bedrock section through the stable rock strata, the influence of pore water pressure change should be fully considered, which is to ensure that the shaft lining not only can take full advantage of deformation and compression effect but also has high bearing capacity.

Data Availability

The data used to support the findings of this study are available from the corresponding author upon request.

Conflicts of Interest

The authors declare that there are no conflicts of interest regarding the publication of this paper.

Acknowledgments

This research was supported by the National Key Research and Development Program of China (2016YFC0600904). The authors would like to thank the editor and reviewers for their contributions on the paper.

References

[1] Z. S. Yao, H. Cheng, and C. X. Rong, "Shaft structural design and optimization of deep freezing," *Journal of China Coal Society*, vol. 35, no. 5, pp. 760–764, 2010.

[2] I. W. Farmer and D. H. Jennings, ""Effect of strata permeability on the radial hydrostatic pressures on mine linings," *International Journal of Mine Water*, vol. 2, no. 3, pp. 17–24, 1983.

[3] J. Bear, "Dynamics of fluids in porous media," *Engineering Geology*, vol. 7, no. 2, pp. 174-175, 1972.

[4] M. S. Bruno and F. M. Nakagawa, "Pore pressure influence on tensile fracture propagation in sedimentary rock," *International Journal of Mining Science and Technology*, vol. 28, no. 4, pp. 261–273, 1991.

[5] R. W. Zimmerman, "Coupling in poroelasticity and thermoelasticity," *International Journal of Rock Mechanics and Mining Sciences*, vol. 37, no. 1-2, pp. 79–87, 2000.

[6] Z. Jiang, S. Feng, and S. Fu, "Coupled hydro-mechanical effect of a fractured rock mass under high water pressure," *Journal of Rock Mechanics and Geotechnical Engineering*, vol. 4, no. 1, pp. 88–96, 2012.

[7] G. D. Lou and L. F. Su, "Analysis of loading on shaft lining subjected to alluvium settlement due to waterdrainage," *Journal of China Coal Society*, vol. 16, no. 4, pp. 54–62, 1991.

[8] W. H. Yang and H. L. Fu, "Theoretical investigation on the vertical additional force of shaft lining in special stratum," *Journal of China University of Mining and Technology*, vol. 9, no. 2, pp. 130–136, 1999.

[9] Y. Wang, C. Zhang, L. Xue, and X. Huang, "Prediction and safety analysis of additional vertical stress within a shaft wall in an extra-thick alluvium," *Mining Science and Technology*, vol. 20, no. 3, pp. 350–356, 2010.

[10] Z. Zhang, X. Tang, and Q. Yu, "Impact of aquifer drainage on shaft lining in underground mining of Eastern China," *Electronic Journal of Geotechnical Engineering*, vol. 21, no. 13, pp. 4721–4729, 2016.

[11] X. Sun, G. Li, C. Zhao, Y. Liu, and C. Miao, "Investigation of deep mine shaft stability in alternating hard and soft rock strata using three-dimensional numerical modeling," *Processes*, vol. 7, no. 1, p. 17, 2019.

[12] R. S. Yang, Q. X. Wang, and S. Z. Chen, "Elactic analysis of irregular inclined shaft lining subjected to water pressure," *Journal of China University of Mining and Technology*, vol. 46, no. 1, pp. 48–57, 2017.

[13] Q. B. Meng, L. J. Han, R. J. Shi et al., "Study and application of construction technology for inclined shafts penetrating drift sand strata in coal mine," *Chinese Journal of Geotechnical Engineering*, vol. 37, no. 5, pp. 900–910, 2015.

[14] O. C. Zienkiewicz, R. L. Taylor, and J. Z. Zhu, *The Finite Element Method: Its Basis and Fundamentals*, Elsevier/Butterworth Heinemann, Amsterdam, Netherlands, 7th edition, 2013.

[15] J. Rutqvist, L. Börgesson, M. Chijimatsu et al., "Thermohydromechanics of partially saturated geological media:govening equations and formulation of four finite element models," *International Journal of Rock Mechanics and Mining Sciences*, vol. 38, no. 1, pp. 105–127, 2001.

[16] C. H. Zhang, F. Jin, Y. L. Hou et al., *Discrete-Contact-Fracture Analysis of Rock and Concrete*, Tsinghua University Press, Beijing, China, 2008.

[17] D. L. Bo, *Hydraulic Load of Underground Structure in Pore Water Bearing Rock*, China University of Mining and Technology, 2015.

[18] S. P. Timoshenko and J. N. Goodier, *Theory of Elasticity*, McGraw-Hill, New York, NY, USA, 1970.

[19] M. O. H. U.-R. D. P. R. China, *Code for Design of Concrete Structures (GB 50010-2010)*, China Architecture & Building Press, Beijing, China, 2015.

[20] C. M. C. A., "Technical Code for Engineering of Ground Anchorages and Shotcrete Support (GB 50086)," Tech. Rep., China Planning Press, Beijing, China, 2015.